universität wien

# BACHELOR THESIS

## Design and implementation of a PIPS detector

intended academic degree

Bachelor of Science (BSc)


| | |
|---|---|
| Author: | Claudia Heindler |
| Matriculation number: | 1207820 |
| Discipline of study: | Physics |
| Supervisor: | Prof. Eberhard Widmann |


Vienna, 26th June 2015

# Abstract

Within the frame work of this Bachelor thesis, a mount for a semiconductor detector - more precisely a PIPS detector - gets designed, constructed and produced. This detector is supposed to work as both a beam blocker and a normalization counter in the antihydrogen spectroscopy experiment of the ASACUSA collaboration at CERN. The aim of this experiment is the measurement of the ground state hyperfine splitting of antihydrogen by a Rabi-method in order to test CPT symmetry and consequently the Standard Model of particle physics. Since the object of investigation is antimatter, the detector and its mount have to satisfy several conditions for ultra-high vacuum. This was concerned when designing the mount of the detector and selecting the materials utilized.



# Zusammenfassung

Im Rahmen dieser Bachelorarbeit wird eine Halterung fr einen Halbleiterdetektor - genauer gesagt einen PIPS Detektor - geplant, produziert und gebaut. Dieser Detektor wird als Strahlblocker und zur Normierung im Antiwasserstoff-Spektroskopie Experiment der ASACUSA Kollaboration am CERN eingesetzt. Ziel dieses Experiments ist die Messung der Hyperfeinaufspaltung des Grundzustandes von Antiwasserstoff mittels Rabi-Spektroskopie um CPT Symmetrie und folglich auch das Standardmodell der Teilchenphysik zu testen. Da im Experiment mit Antimaterie gearbeitet wird, mssen der Detektor sowie seine Halterund einige Bedingungen fr Ultrahoch-Vakuum erfllen. Das wurde bei der Planung der Halterung und der Auswahl der Materialen bercksichtigt.

# Contents

# 1 Theoretical Background and Motivation

## 1.1 CPT symmetry

In 1955, the CPT theorem - where C stands for charge conjugation, P for parity transformation and T for time reversal - offered a theoretical base for the concept of matter-antimatter symmetry [15]. According to CPT symmetry the properties of particles and their antiparticles are either exactly the same or exactly the opposite [4].

In the Standard Model of particle physics, this symmetry is conserved. In order to probe the limits of the Standard Model of physics, scientists aim to test CPT invariance. Therefore, antihydrogen ($\bar{H}$) and hydrogen ($H$) are ideal candidates for investigation as antihydrogen is the simplest antiatom and hydrogen the most precisely investigated system in physics. If any difference between these two systems was measured, CPT symmetry would have been shown to be violated and additional physics beyond the Standard Model would have been discovered.[13] The high sensitivity for such discoveries in $H$ and $\bar{H}$ arises from the possibility to apply precise spectroscopy methods. [21]

As the ground state hyperfine splittings (GS-HFS) of the two atoms are directly sensitive to CPT violating terms, the ASACUSA (Atomic Spectroscopy And Collisions Using Slow Antiprotons) collaboration aims to measure the GS-HFS of $\bar{H}$ in order to compare it with the one of $H$ [13]. According to Hellwig [10], for hydrogen the frequency of the ground state hyperfine splitting $\nu_{GS-HFS}$ measured with MASER spectroscopy is

$$\nu_{GS-HFS}(H) = (1420405751.768 \pm 0.002)Hz \tag{1.1}$$

## 1.2 Hyperfine splitting in Hydrogen and Antihydrogen

The hyperfine structure is the splitting of the atomic energy levels as a consequence of the interaction of the proton's - or in general the nucleus' - magnetic moment with the magnetic moment of the atomic shell. In the case of hydrogen the total angular momentum of the atom $\vec{F}$ is the sum of the proton's spin $\vec{I}$ and the electron's angular momentum $\vec{J}$:

$$\vec{F} = \vec{I} + \vec{J} \tag{1.2}$$

For the ground state of hydrogen this gives two possible values for $F$ as $J = s = \frac{1}{2}$ (where $s$ is the spin of the electron) and $I = \frac{1}{2}$. This leads to $F = \frac{1}{2} \pm \frac{1}{2}$. Therefore, $F = 0$ if the two spins are antiparallel and $F = 1$ if the two spins are parallel [17, p.107ff.].

A complete description of the state of the atom is given in the basis $|F, M\rangle$ where $F$ is again the total angular momentum of the atom and $M$ is the third component.

For leading order CPT violating effects, one considers $H$ and $\bar{H}$ confined by external trapping fields. Those allow avoidance of suppression effects of CPT violating terms and separation of different spin states according to the so called Zeeman effect [21].

### 1.2.1 Zeeman effect

An external magnetic field $B$ leads to a splitting of the spectral lines of an atom due to the interaction of the magnetic moment with this magnetic field. [2, p.45]. At $B = 0$ the triplet state (F=1) is degenerated [21].

The states $(F, M) = (1, 1)$ and $(F, M) = (1, 0)$ are called low field seekers (LFS) as the energy of these states is increasing in the presence of an external magnetic field. Atoms in these states experience a force towards regions of lower magnetic field. In opposite to that $(F, M) = (1, -1)$ and $(F, M) = (0, 0)$ are called high field seekers (HFS) because of their decreasing energy in regions of higher magnetic field. Therefore, those states are spatially deflected to regions of higher magnitude of $B$ [4].

The detectable transitions in a Rabi-like experiment (see chapter 2.1) are those between high and low field seeking states. The transition with $\Delta M = 0$ is the $\sigma$-transition which has only a second order magnetic field dependence at low magnetic field strengths. The transitions with $\Delta M = \pm 1$ are the $\pi$-transitions and have first order B-field dependence. [9, p.219]. Diagram 1.1 shows the Zeeman effect for antihydrogen including the transitions:

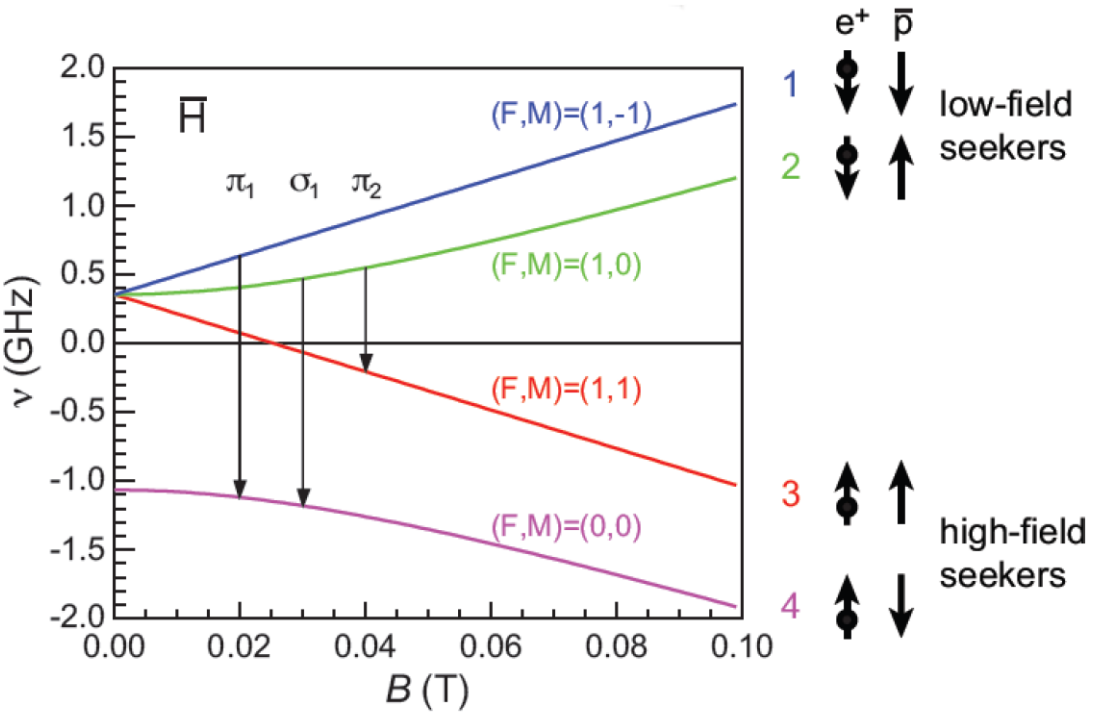


**Figure 1.1:** Breit-Rabi-diagram for antihydrogen with positron ($e^+$) and antiproton ($\bar{p}$) spin adjustement: (F,M)=(0,0) is the singlet state and (F,M)=(1,1),(1,0),(1,-1) is the triplet state. The transition (1,-1) $\rightarrow$ (0,0) is called $\pi_1$, (1,0) $\rightarrow$ (1,-1) is called $\pi_2$ and (1,0) $\rightarrow$ (0,0) is called $\sigma_1$ [4],[9, p.219].

# 2 Experimental Setup

In the antihydrogen experiment conducted by the ASACUSA collaboration at CERN's Antiproton Decelerator (AD), the GS-HFS of antihydrogen shall be measured by Rabi-like spectroscopy [13].

## 2.1 The Rabi method

The Rabi spectroscopy is based on polarized atomic beams [13]. With help of external magnetic fields, spin states are spatially separated (see 1.1) as a particle with magnetic moment $\vec{\mu}$ feels a force $\vec{F}$ if a magnetic field gradient $\vec{\nabla}\vec{B}$ is applied:

$$\vec{F} = \vec{\nabla}(\vec{\mu}\vec{B}) \tag{2.1}$$

The Rabi method consists firstly of a magnetic field gradient which generates a spin polarized beam followed by an oscillating magnetic field to drive spin flips (transitions). In the end a second magnetic field gradient is placed to select spin states which did not undergo a transition. This leads at the end to a drop in the count rate of the detector when spin flips are occurring. According tu Kusch [14], for hydrogen the frequency of the ground state hyperfine splitting $\nu_{GS-HFS}$ measured with Rabi-like spectroscopy is

$$\nu_{GS-HFS}(H) = (1420.405753 \pm 0.00005)MHz \tag{2.2}$$

In the experiment for antihydrogen, the first B-field gradient is implemented in the cusp trap - the formation region of antihydrogen. The oscillating B-field is generated by an oscillating microwave field in a cavity with a frequency of about 1.42 GHz. The states are then analyzed by a sextupole magnet [4].

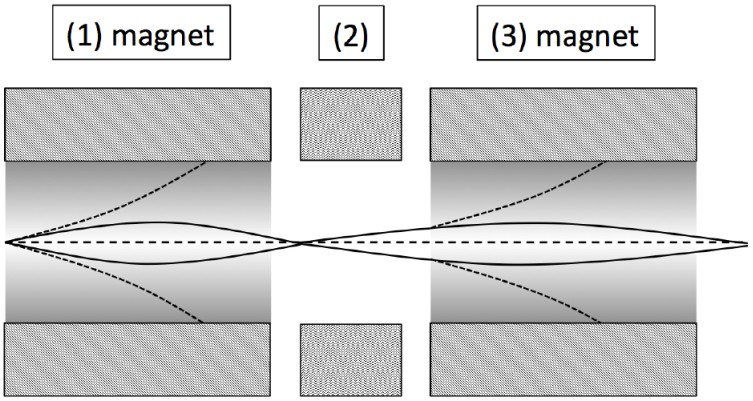


**Figure 2.1:** Rabi-method: In magnet (1) - implemented in the cusp trap - the beam gets polarized by selecting the spin states. In (2) the oscillating B-field drives the spin flips - a microwave cavity in the experiment - and the magnet in (3) - a sextupole - analyzes the states [4].

## 2.2 The Antihydrogen Setup

Figure 2.2 gives an overview of the beamline of the experiment and its constituents.

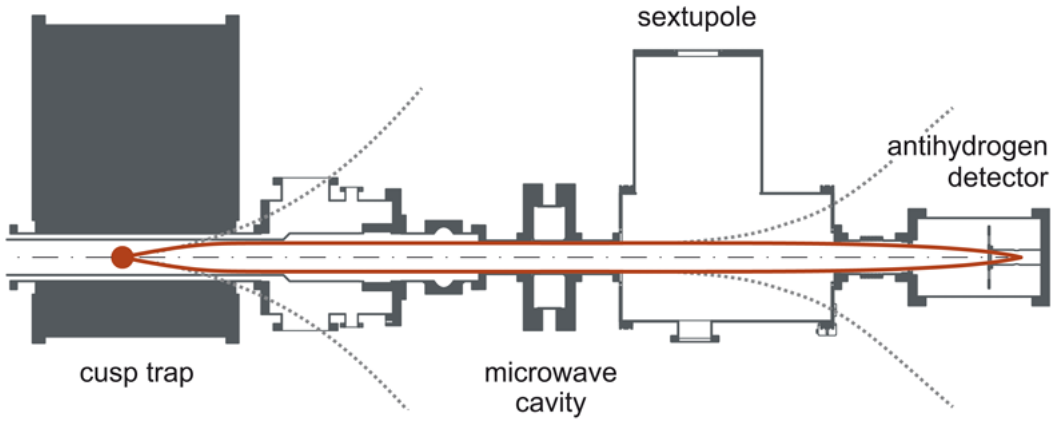


**Figure 2.2:** In the cusp trap, LFS (solid lines) and HFS (dashed lines) of $\bar{H}$ atoms are formed. LFS states are focused, in the cavity a spin flip is driven. The sextupole then analyzes the spin states by defocusing the generated HFS states. The detector shows a drop in count rate [22].

### 2.2.1 The cusp trap

For measuring the GS-HFS of $\bar{H}$, a spin-polarized beam, which is provided by the cusp trap, is essential for the ASACUSA experiment. This trap consists of a superconducting anti-Helmholtz coil and multiple ring electrodes [5, p.1]. The coil leads to a magnetic quadrupole field with axial symmetry about the coil axis (see figure 2.3). The multi-ring electrodes form an axially symmetric electric field [25]. As a consequence, stable storage of antiprotons and positrons is provided in a so-called nested trap potential. Consequently, antiprotons and positrons can be mixed and start forming neutral $\bar{H}$ atoms. These neutral atoms are no longer trapped by the electromagnetic fields and therefore escape the cusp trap. $\bar{H}$ atoms which are in the low field seeking (LFS) states get focused during escaping because of the minimum value of the B field along the central axis. In opposite to that, HFS states are defocused as the magnitude of the B field increases outwardly. The result is a spin-polarized beam of $\bar{H}$ atoms [5].

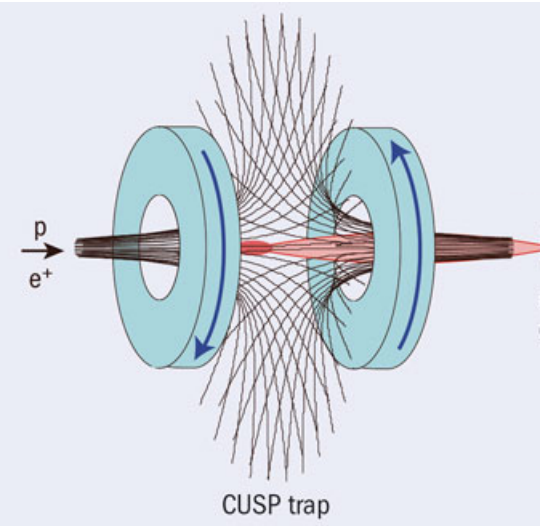


**Figure 2.3:** Positrons and antiprotons are injected into the cusp trap. The anti-Helmholtz coil forms a magnetic quadrupole field. A beam of spin-polarized antihydrogen (LFS state) is emitted. [5]

### 2.2.2 The microwave cavity

In the microwave cavity the spin flips are induced by a radio frequency field. The geometry of the cavity is optimized to the GS-HFS frequency $\nu_{GS-HFS}$ of about 1.42 GHz. This radio frequency field is superimposed by a static magnetic field created by a Helmholtz coil in order to prevent spontaneous spin flips - so called Majorana spin flips [6]. Depending on the orientation of the RF field with respect to the static magnetic field, either $\sigma$ or $\pi$ transitions are driven [16]. In either case the polarization of the $\bar{H}$ beam changes from LFS to HFS, which allows for a subsequent detection of the spin-flip.

Furthermore, the cavity is shielded against fringe fields from the cusp trap as well as those from the sextupole magnet to ensure homogeneity of the field inside the cavity [6].

### 2.2.3 Detecting antihydrogen

Antihydrogen can be detected by means of antiproton and positron annihilation with matter [23, p.16]. If an antiproton annihilates with material from the detector, on average two neutral pions and three charged pions are produced [1].

The $\bar{H}$ detector in the experiment is in principle a scintillation detector which is made out of a bismuth germanium oxide (BGO) single-crystal placed in a magnetic field-free region [13]. Such a detector has in general two major components: a scintillating material connected with a photomultiplier by a light guide. An incoming particle excites the atoms of the scintillating material. The excited atoms then re-emit the absorbed energy in form of photons which are passed to the photomultiplier tubes by light guides. There, a particle shower of electrons is produced which leads to a measurable pulse at the end of the photomultiplier tube [8, p.63].

Because of its high density, high photon yield and ultra-high vacuum (UHV) compatibility, BGO was chosen as scintillating material for the detector in the experiment [13]. Surrounding the vacuum chamber which encloses the BGO, 2 times 32 plastic scintillator bars are assembled in a detector hodoscope geometry [16] in order to track annihilation pions. An important point is reducing unwanted background events primarily caused by cosmic rays. This is done by only counting coincidence events between the BGO and the plastic scintillators and by applying cuts to additional information provided by the detector as for instance the energy deposit on the BGO or time correlations between different scintillator bars on the Hodoscope. [13].

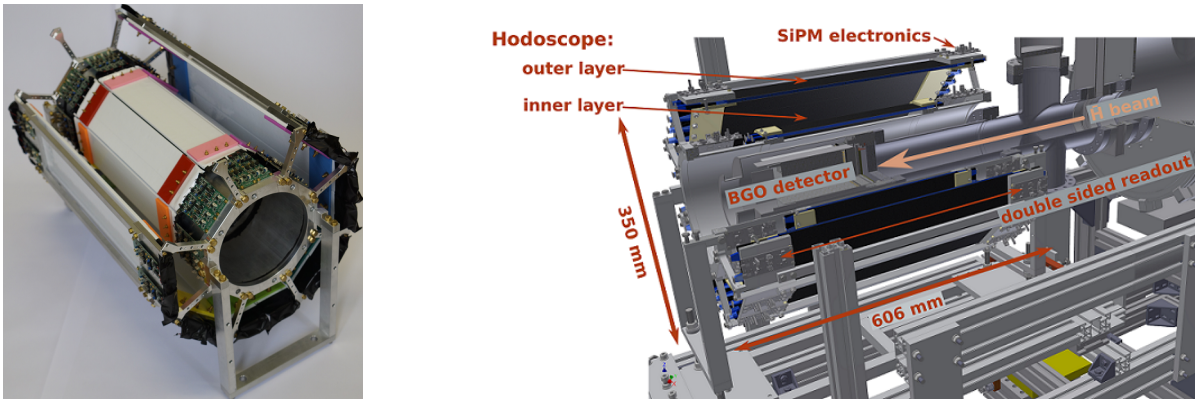


(a) (b)

**Figure 2.4:** (a): Surrounding plastic scintillators. (b): Drawing of the whole detector with BGO inside, surrounded by two layers of scintillators, read out by the silicon photomultipliers (SiPM electronics)

### 2.2.4 Additional diagnostics tools

The vacuum chamber between the cusp trap and the microwave cavity houses additional beam diagnostics:

- field ionizer
- beam blocker
- normalization counter

The field ionizer is capable of removing highly exited $\bar{H}$ atoms (so-called Rydberg-states with principal quantum number $n > 12$), which are not useful for ground-state spectroscopy. $\bar{H}$ atoms which are not in the ground-state but too tightly bound to be ionized have good chances to decay to the ground-state while traveling from the field ionizer to the microwave cavity. The beam blocker, which should be removable, is needed in order to block the antihydrogen atoms with trajectories close to the center of the flight line. There the B-field gradient of the analyzing sextupole magnet is weak and the inability to separate LFS and HFS states appropriately would lead to a background signal when detecting the antihydrogen atoms. The normalization counter shall produce a reference signal which is proportional to the incoming rate of $\bar{H}$ atoms. The count rate at the antihydrogen detector at the end of the beamline can then be normalized to this signal. As a drop in count rate will be the indicator for spin-flips, it is important to exclude other reasons for such a drop.

The $\bar{H}$ atoms annihilating on the beam blocker are ideally suited to serve as a reference signal for the amount of incoming particles. Initially, such annihilation events have been counted by scintillator bars outside the vacuum chamber only. By making the beam blocker an active component, the annihilation becomes directly detectable. By using coincidences with the scintillator bars, a good background suppression can be accomplished.

Within the frame work of this Bachelor thesis, it was decided to use a special semiconductor detector (see chapter 3.1) made out of silicon - a so-called PIPS detector (Passive Implanted Planar Silicon) for this purpose. This detector therefore serves at the same time as a beam blocker and normalization counter. This allows converting the annihilation events into an electric signal, which makes it easier to run the signal along the movable component and out of the vacuum chamber. Furthermore, such a detector meets the ultra-high-vacuum conditions. Thus, the beam blocker will be replaced by the PIPS detector.

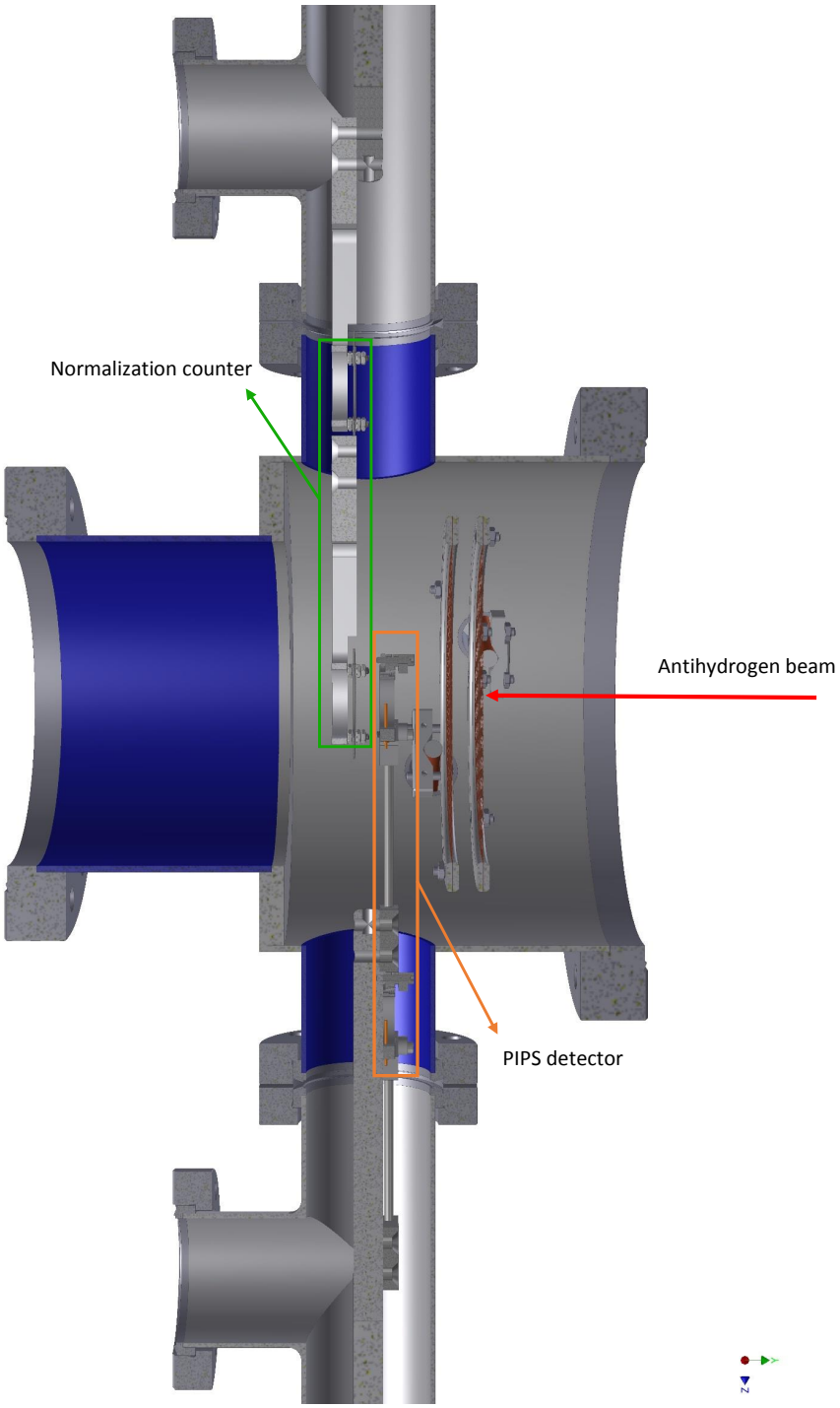


**Figure 2.5:** Vacuum chamber including the normalization counter installed so far and the PIPS detector (instead of the passive beam blocker) as well as the field ionizer.

# 3 The PIPS detector

A PIPS detector is a type of semiconductor detector. The working principle is described briefly below in chapter 3.1. The one which will be implemented in the experiment has the form of an octagon (see figure 5.2 for the physical dimensions) and will serve as an active beam blocker.

While it has the same detector element as the currently installed normalization counter, it will block a significantly smaller area of the antihydrogen beam as the whole detector mount is custom made at the SMI (Institute for Subatomic and Atomic Physics). In contrast, for the first normalization counter the same detector element is already attached to a larger ceramic ring and commercially available in this combination.

The passive beam blocker will get replaced by this custom made PIPS detector with the smaller blocking cross section (more details in chapter 3.2).


**Figure 3.1:** PIPS detector PD 300-300 of the company Canberra

## 3.1 Semiconductor detectors

The functional principle of a semiconductor detector is the formation of electron - hole pairs by charged particles passing through the semiconducting material. The amount of the formed ion pairs $n_{ion}$ is given by:

$$n_{ion} = \frac{E_c}{W} \tag{3.1}$$

where $E_c$ is the energy of the charged particle and $W$ the required energy for forming an ion pair. Commonly used semiconducting materials for such a detector are germanium and silicon. For the latter $W = 3.5$ eV. [8, p.70] These materials get doped with donors and acceptors in order to produce a p-doped and a n-doped semiconductor layer. If

these layers are in contact, electrons diffuse from the n-doped layer into the adjoined layer and vice versa (shown in figure 3.2 (1) ). Because of partial compensation of charges a positive space-charge of unmovable donors and a negative space-charge of unmovable acceptors results in the n-doped layer and in the p-doped layer, respectively. Thus, a depletion layer forms. The resulting electric field prevents further diffusion (see figure 3.2 (2) ).

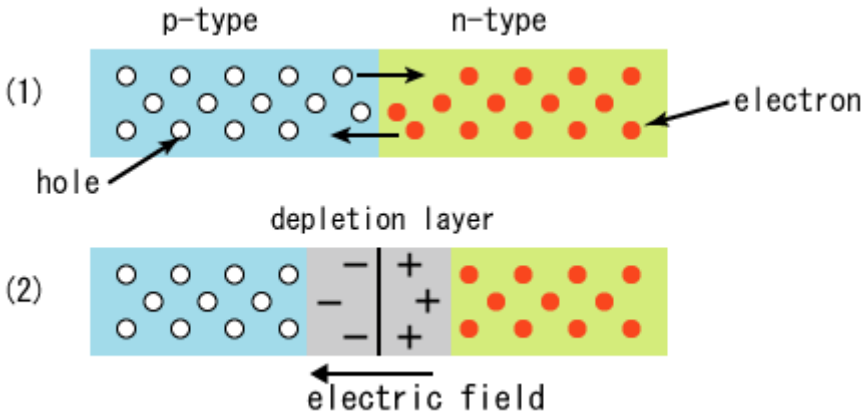


**Figure 3.2:** (1): p- and n-doped layer where electrons and holes start to diffuse. (2): formation of a depletion layer.[24]

Applying an external voltage difference in reverse direction (cathode at p-doped layer and anode at n-doped layer), the depletion layer gets broadened. As a consequence, no current can be measured. However, if a charged particle crosses the space charge region, electron-hole pairs are created. This leads to a measurable signal as they start drifting to the anode/cathode. [20, p.159f.]

## 3.2 Design and construction of the mount for the PIPS detector

### 3.2.1 Electronics and signal read out

As described in chapter 3.1, an external voltage is applied at the detector. According to the manufacturing company CANBERRA, for the PIPS this voltage is $U = 60$V. The electrical signal will be established by bonding wires to the junction of the detector. These wires are then guided outside the vacuum chamber through electrical feedthroughs and connected to a pre-amplifier which is needed in order to stabilize the signal and - in case - also for amplification. The ultrasonic wire bonding is done because of the UHV conditions. Soldering and welding would not only produce too much impurities but also contain outgassing materials. The bonding can only be done with special machines. Therefore colleagues from HEPHY (Institute for high energy physics) were contacted

in order to bond the PIPS detector with their bonding machine. The ultrasonic wire bonding is a process which is mainly used to electrically connect integrated circuits to circuit packages [12]. It is executed at room temperature. This is possible because ultrasonic energy leads to changes in morphology equivalent to those produced with high heat. Therefore it causes less damage to the bond pad than other methods. [3, p.1f.] One thing which has to be considered when designing the mount of the detector is the sensitivity of the bonding contacts.

### 3.2.2 Materials for the mount

The demands for the mount of the PIPS detector are ultra-high vacuum capability ( $\leq 10^{-10}$ mbar) and electric insulation. According to these requirements, several materials for the mount were considered, amongst others MACOR (glass ceramics), PEEK (polyetheretherketone, a synthetic aromatic linear polymer) and VESPEL (polymide-based plastics).

Finally, PEEK was chosen, as the outgassing of VESPEL is five times higher than that of PEEK [19]. According to gaschromatographic-mass spectrometer analysis the outgassing of PEEK is compatible with the requirements for UHV [18]. The other main advantage of this material is its lower cost despite its good dimensional stability and machine characteristics as well as dielectric strength. Furthermore it shows an excellent creep resistance at increased temperature as well as wear and abrasion resistance [19].

### 3.2.3 Size and shape of the mount

In order not to lose too many $\bar{H}$ atoms when blocking the center of the beam, the mount for the detector has to be as small in cross-section area as possible. Therefore, it was decided to put the detector onto a mount of PEEK material which is in cross-section area not much bigger than the detector itself. Furthermore, the physical dimensions of the mount are constricted by the available space in the vacuum chamber, in which the detector is going to be placed. Besides, the bonding contacts are very sensitive.

This led to the first design for the mount, shown in figure 3.3 (a). The PIPS detector is fixed on four corners by cylinder-head screws. The detector does not overlie directly on the PEEK material but is rested on a ring which is placed on eight gold springs in order to prevent the detector from damage through mechanical forces. The detector is therefore fixed on the mount by the spring forces of the gold springs - the fixing does not depend on the torque with which the screws get tightened. Two threaded rods connect the PEEK material with the lower stainless steel mount. The threaded rods as well as the four screws get extra holes to vent trapped volumes. The contacts for bonding are placed on the bottom edge of the detector between the threaded rods in order to protect them against mechanical damage. On this bottom edge, two holes will be drilled through the PEEK material for putting gold pins into them. The bonding will establish the electrical connection between the detector and the pins. On the other side of the pins wires will be connected by spot-welding them. These wires will be guided down to

the stainless steel mount along the threaded rods in order to keep the whole design very compact.

In a second design iteration, shown in figure 3.3 (b), small modifications have been introduced to further minimize the cross-section area of the mount: The holes for the gold pins will be drilled through the PEEK parallel to the detector and the PEEK material gets milled out around the screws in order to minimize the cross section area even more. Furthermore, the detector gets mounted on three corners instead of four. The eight gold springs are reduced to three, one spring at each screw.

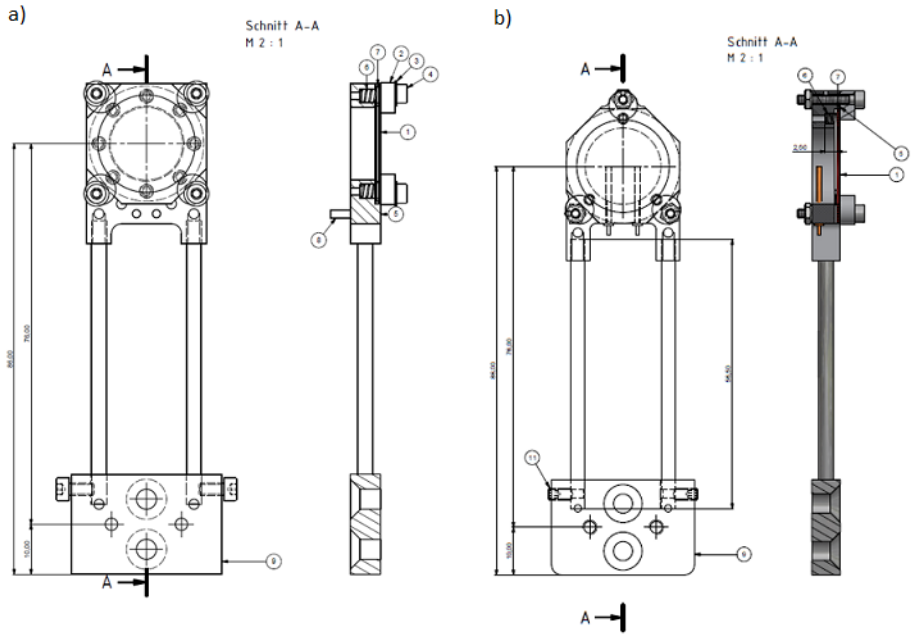


**Figure 3.3:** a): Engineering drawing of the first design of the PIPS mount. b) Second design.

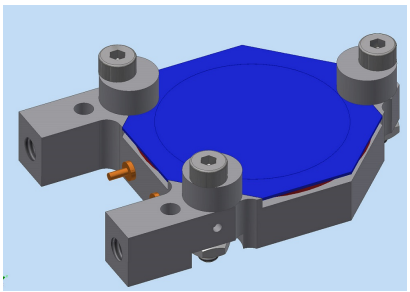

**Figure 3.4:** CAD drawing of the second design of the mount for the PIPS detector

With equal active detector area, this design gives so far a reduction in cross-section

area by a factor of about 1.38 which is an improvement of $\sim 20\%$. Figure 3.5 shows a schematic sketch of the cross section of the vacuum chamber housing the detectors:

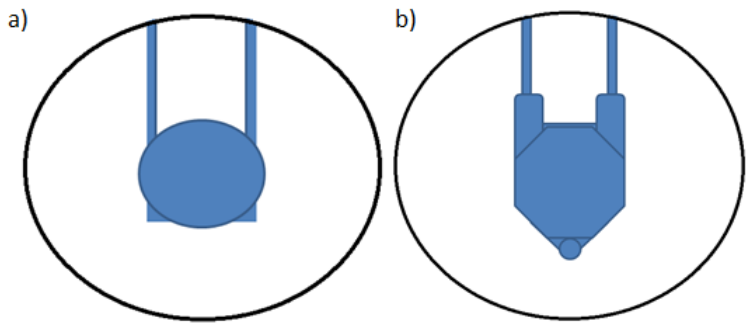


**Figure 3.5:** Schematic sketch of the cross section of the vacuum chamber: a) housing the so far implemented PIPS, b) housing the one which is currently going to be built.

Table 3.1 shows a comparison of the cross section areas of the implemented PIPS detector and the new one referenced to the cross section area $A_{vc}$ of the spectroscopy beamline of inner diameter $d = 100$ mm and $A_{vc} = d^2 4\pi \approx 7854$ mm$^2$. Furthermore, the gain in area both in absolute and relative value has been calculated.

| | Area [mm$^2$] | Blocked area relative to $A_{vc}$ in % |
|---|---|---|
| Implemented PIPS | 871 | 11.1 |
| New PIPS | 695 | 8.8 |
| Absolute and relative gain in area | 176 | 20.2 |

**Table 3.1:** Calculations of the cross section areas of the implemented and the new PIPS as well as comparisons in absolute and relative value.

After ensuring that this is the minimal area possible for the mount of the detector, the second design was then sent to physicists from HEPHY to receive their agreement whether bonding was possible. Additional to their approval, it was suggested to drill screw threads directly into the PEEK material instead of using screw nuts. In order to quantify the stability of M2.5 (diameter of 2.5 mm) and M2 (diameter of 2 mm) threaded holes in PEEK a test was performed. Two M2 and two M2.5 screw threads were drilled through a 6 mm thick layer of PEEK material. Using a torque wrench the maximal applicable torque $M_{max}$ was determined.

The results are listed in table 3.2:

| **screw thread** | M2 | | M2.5 | |
|---|---|---|---|---|
| **thread number** | 1 | 2 | 1 | 2 |
| $M_{max}$ [Ncm] | 54 | 64 | 80 | 75 |

**Table 3.2:** M2 and M2.5 thread tests in PEEK material. $M_{max}$ is the maximal applicable torque.

As a consequence of these results, it was decided to drill a M2 screw thread into the PEEK mount in which the screws get tightened with a maximum torque of $M_{max} = 35$ Ncm. Thereby the screws are screwed strong enough while at the same time the threads are not destroyed.

Besides, it was taken into account that the wires which get spot-welded on the gold pens have to be guided down along the screw threads. In order to ensure that the wires do not need to much space, it was decided to shift one of the holes for the gold pens. This leads to sufficient place for a third hole, through which the wires can be guided. Thus, the third and final design, shown in figure 3.6, for the mount of the PIPS was created:

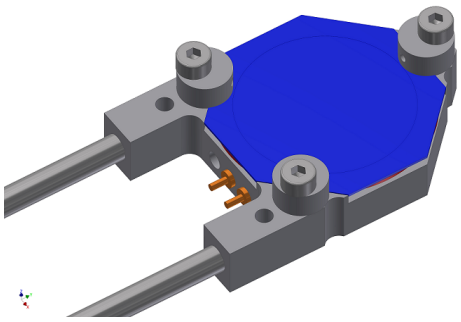

**Figure 3.6:** CAD drawing of the final design of the mount for the PIPS

## 3.3 Assembling the detector

### 3.3.1 Test assembly

Before continuing manufacturing the mount for the PIPS detector, a first test assembly was done to ensure that the detector fits onto the mount. Therefore, the mount was cleaned for UHV conditions in order to avoid contaminating the detector. (Cleaning the latter would be much more complicated and sensitive than cleaning the PEEK mount.) For this test assembly, acids were avoided, as according to AHLBORN KUNSTSTOFFE E.U. [7] and KERN GmbH [11], PEEK is not stable to several acids. Thus, acetone was used during the cleaning process. The cleaning process was done in several steps:

1. Cleaning the PEEK mount with water and soap.

2. Inlaying it into 5% soap solution and cleaning it in the ultrasonic bath at a temperature of about 50°C for 15 minutes.
3. Flushing the mount with water.
4. Repeating Step 2 with water instead of soap solution.
5. Step 2 again with acetone.
6. Flushing with deionized water and Step 2 again with deionized water.
7. Putting the mount in the oven for half an hour at 100 $^{circ}$C.

After these steps, the PIPS detector was very carefully put onto the PEEK mount which perfectly fitted for the detector, as shown in figure 3.7:

**Figure 3.7:** Test assembly of the PIPS detector and its mount

Therefore, the construction of the mount and all its components continued.

# 4 Conclusion and outlook

Within the frame work of this Bachelor thesis, a mount for the PIPS detector, which will serve as a beam blocker and normalization counter in the antihydrogen spectroscopy experiment, was designed. Requirements on the mount were UHV capability and a minimal cross-section area. Under several materials, the plastic PEEK was chosen for the mount because of its outgassing properties. During the design and construction progress, tests in material properties and cleaning for UHV conditions were done. So far, the PEEK mount was constructed and the PIPS detector fits onto the mount. The manufactured and delivered components have been cleaned according to UHV conditions. The electrical connections both the bonding and the spot-welding have to be done yet. After that, tests with a radioactive source are planned. The last step is going to be the mounting of the PIPS detector at the antihydrogen spectroscopy experiment at CERN.

# List of Figures

# List of Tables

# Bibliography


[1] Andresen G.B. et al. Antihydrogen annihilation reconstruction with the ALPHA silicon detector, 14 Jul 2011.

[2] Broecker Bernhard. *dtv-Atlas Atomphysik*. 1976 Deutsch Taschenbuch Verlag GmbH & Co. KG, München, München.

[3] Chauhan P.S. et al. *Copper Wire Bonding*. Springer New York Heidelberg Dordrecht London, 2014.

[4] Diermaier M. et al. An atomic hydrogen beam to test ASACUSA's apparatus for antihydrogen spectroscopy, 12 Jan 2015.

[5] Enomoto Y. et al. Synthesis of cold antihydrogen in a cusp trap, 10 Dec 2010.

[6] Federmann S. et al. Design of a 1.42 GHz Spin-flip cavity for antihydrogen atoms.

[7] Firma Ahlborn Kunststoffe. Chemische Eigenschaften peek.

[8] Frauenfelder H., Henley E.M. *Teilchen und Kerne: Subatomare Physik*. R. Oldenbourg Verlag GmbH, München, 2. edition.

[9] Haken Hermann, Wolf Hans Christoph. *Atom- und Quantenphysik. Einführung in die experimentellen und theoretischen Grundlagen.* Springer-Verlag Berlin Heidelberg New York, 8. edition.

[10] Hellwig Helmut et al. Measurement of the Unberturbed Hydrogen Hyperfine Transition Frequency, Nov 1970.

[11] Kern GmbH Web Communications. Polyetheretherketon: Chemische Eigenschaften.

[12] Krzanowski J.E. A transmission electron microscopy study of ultrasonic wire bonding, March 1990.

[13] Kuroda N. et al. A source of antihydrogen for in-flight hyperfine spectroscopy, 21 Jan 2014.

[14] Kusch P. Redetermination of the Hyperfine Splittings of Hydrogen and Deuterium in the Ground State, 12 Aug 1955.

[15] Landua R. Antihydrogen at CERN, 2004.

[16] Malbrunot C. et al. Spectroscopy apparatus for the measurement of the hyperfine structure of antihydrogen, 2014.

[17] T. Mayer-Kuckuk. *Atomphysik. Eine Einführung.* Teubner-Studienbücher: Physik, Stuttgart, 5. edition, 1997.

[18] Murari A., Barzon A. Comparison of new PEEK seals with traditional helicoflex for ultra high vacuum applications, 25 Aug 2003.

[19] Murari A. et al. Comparison of PEEK and VESPEL SP1 characteristics as vacuum selas for fusion applications, 19 July 2001.

[20] Musiol G. et al. *Kern- und Elementarteilchenphysik.* Verlag Harri Deutsch, Frankfurt am Main, Thun, 2. revised edition, 1995.

[21] Russell N. Investigating Lorentz and CPT Symmetry with Antihydrogen, 2002.

[22] Widmann E. et al. Description: Methodology, 2012.

[23] Widmann E. et al. Measurement of the antihydrogen hyperfine structure: Letter of intent for AD, 25 Feb 2003.

[24] Wikimedia Commons. Introduction to Inorganic Chemistry/Electronic Properties of Materials: Superconductors and Semiconductors.

[25] Yamazaki Y. At the cusp in ASACUSA, 23 Feb 2011.

# 5 Appendices

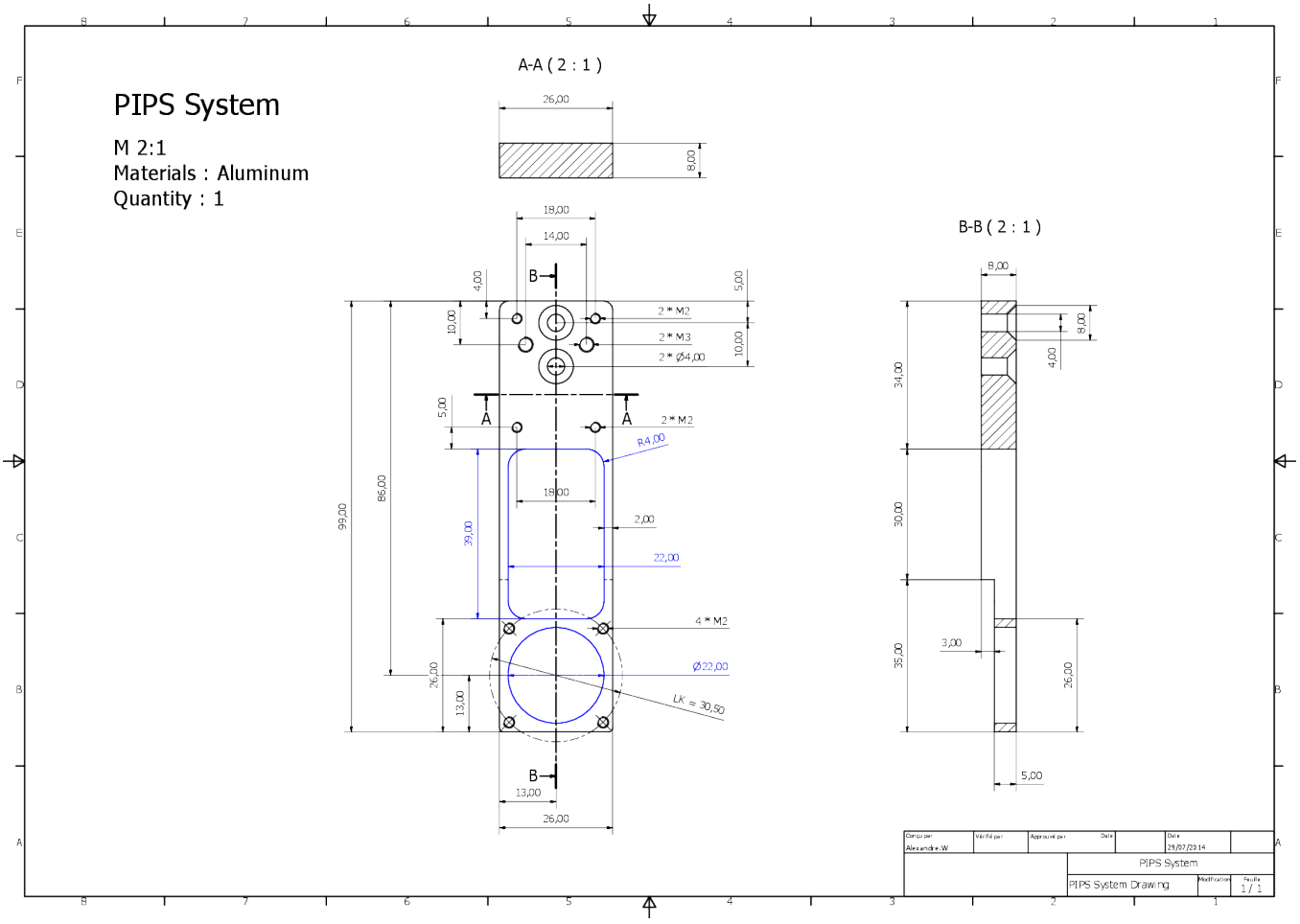


**Figure 5.1:** Engineering drawing of the PIPS detector so far installed at the experiment

| Nominal active area | | Total junction area | | Active area thin window | | Shape | Flat to flat | Min in mount |
|---|---|---|---|---|---|---|---|---|
| mm² | ϕ mm | mm² | ϕ mm | mm² | ϕ mm | | mm | mm |
| 300 | 19.5 | 377 | 21.9 | 314 | 20 | octagon | 24 | 26.0 |

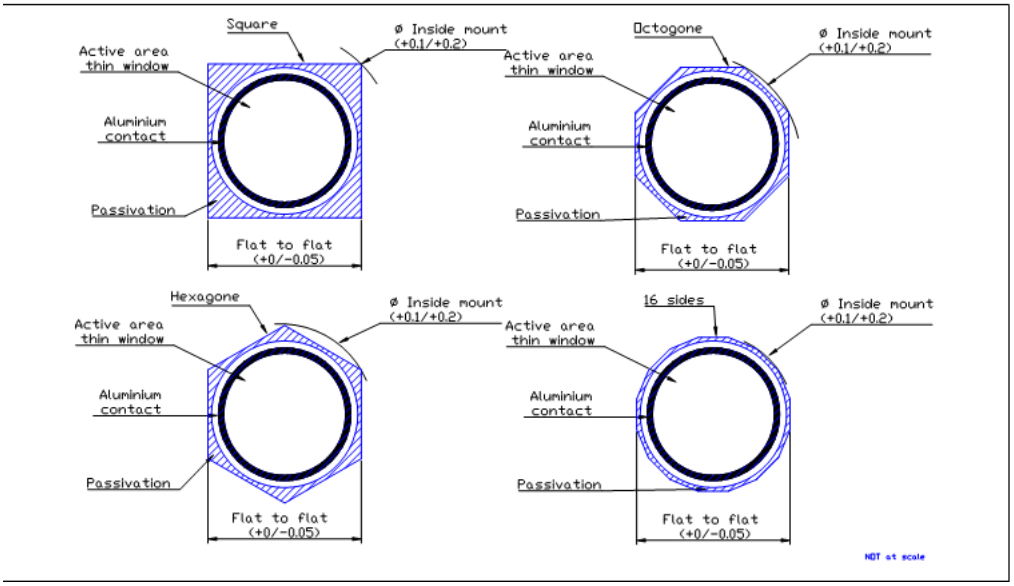


**Figure 5.2:** Physical dimensions of the different PIPS detector models. The octagone is the one at hand.